

# Laser-Mediated Programmable N Doping and Simultaneous Reduction of Graphene Oxides

Li Guo, Yong-Lai Zhang,\* Dong-Dong Han, Hao-Bo Jiang, Dan Wang, Xian-Bin Li, Hong Xia, Jing Feng, Qi-Dai Chen, and Hong-Bo Sun\*

As a rapidly rising star on the horizon of materials science and modern physics, graphene is promising for future nano-electronics due to its exceptional properties including ultra-high carrier mobility, optical transmittance, high conductivity, flexibility, and excellent stability.<sup>[1]</sup> However, the absence of a bandgap in intrinsic graphene sets a huge obstruction for most electronic applications, such as field-effect transistors (FETs),<sup>[2]</sup> sensors,<sup>[3]</sup> and photodiodes.<sup>[4]</sup> Consequently, the demands on universal techniques that could be employed in opening and tuning an energy gap of graphene become more and more critical. In recent years, as the motivation for preparing semiconducting graphene has continued to intensify, rapid progress has been made in this dynamic field. Typically, graphene could be made into semiconductors through two main approaches: one is nanostructuring and the other is heteroatom doping. The former method resorts to making graphene nanostructures such as nanoribbons,<sup>[5]</sup> nanomesh,<sup>[6]</sup> and quantum dots.<sup>[1a]</sup> An energy bandgap would form due to the quantum confinement of electrons, when the size of graphene is structured into narrow geometries (e.g., sub-10 nm). Alternatively, a second route controls the semiconducting properties of graphene by doping with heteroatoms, such as B and N.<sup>[7]</sup> For instance, N-doping has been widely used to tailor the properties of graphene and render it useful for various applications.<sup>[8]</sup> From the practical point of view, N-doping of graphene seems much more feasible when compared with nanostructuring method, which requires ultra-high resolution of graphene geometries. More importantly, the dopant atoms can not only open the energy gap, but also tune the carrier type of graphene in a controlled manner, contributing to the potential use of up-and-coming graphene in various electronic devices.

As representative examples, Wei et al. reported the synthesis of N-doped graphene by chemical vapor deposition (CVD) in the presence of NH<sub>3</sub>,<sup>[9]</sup> where the electrical properties of graphene were effectively modulated through the substitutional

N-doping; Y. W. Zhang reports a feasible direct-synthesis method for preparing N-graphene with a manageable N content on a large scale;<sup>[8a]</sup> Dai's group<sup>[10]</sup> successfully developed a N-doped graphene by high-power electrical annealing of graphene nanoribbons (GNRs) in NH<sub>3</sub>, and the resultant N-species edge-terminated GNRs show n-type transistor behavior. However, the N-atom substitution occurs easily at the edges where there exist plenty of defects and dangling bonds; for pristine graphene, which possesses perfect honeycomb structure, the substitution of sp<sup>2</sup> carbon atoms with heteroatoms becomes more difficult. In this regard, Guo et al.<sup>[11]</sup> reported the generation of in plane defects on graphene sheets by N<sup>+</sup>-ion irradiation; nitrogen atoms could be effectively doped during NH<sub>3</sub> annealing. Using this N-doped graphene, n-type FETs have been successfully fabricated at room temperature.

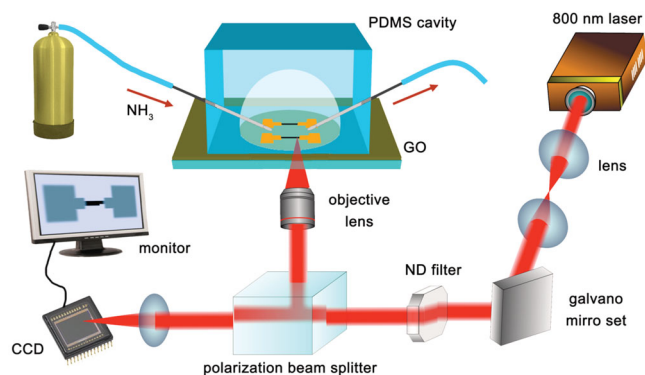
Considering the fact that graphene oxide (GO) possesses plenty of natural oxygen-containing defects that could be restored through proper reduction, GO could be considered an appealing alternative for the purpose of preparing N-doped graphene. Additionally, in view of the mass-production and solution-processing capability, the use of GO would undoubtedly facilitate the fabrication of graphene-based devices. In a standard work, Li et al.<sup>[12]</sup> reported the mass production of N-doped graphene by simultaneous N doping and reduction of GO through a thermal annealing process in ammonia atmosphere. Later, Kumar et al.<sup>[13]</sup> reported the simultaneous reduction and nitrogen doping of GO nanosheets for gram-scale preparation of N-doped graphene using a downstream microwave plasma source. However, although the above-mentioned works have already shown the possibility of doping graphene with nitrogen, usually by treating GO in NH<sub>3</sub> atmosphere, there is still a lack of research that mainly deals with patternable N-doping of graphene towards device fabrication and integration.

As a high power-density optical energy source, a laser is capable of processing graphene and related materials in a controlled manner.<sup>[14]</sup> Previously, the laser-mediated photoreduction of GO reported by our group<sup>[15]</sup> and others<sup>[16]</sup> has already proved its value in the controllable reduction and flexible patterning of GO. However, efforts have been mainly devoted to the reduction of GO in order to partly restore the sp<sup>2</sup> domains and recover their conductivities. Less attention has been paid to simultaneous reduction and heteroatom doping of GO, despite some photoreduction strategies providing not only exquisite control over the oxygen content but also the compatible processing flow with the state-of-the-art of technologies used for device fabrication. To date, the tuning of the energy gap of graphene by heteroatom doping through an optical manner is still

L. Guo, Dr. Y.-L. Zhang, D.-D. Han, H.-B. Jiang,  
D. Wang, Dr. X.-B. Li, H. Xia, Prof. J. Feng,  
Prof. Q.-D. Chen, Prof. H.-B. Sun  
State Key Laboratory on Integrated Optoelectronics  
College of Electronic Science and Engineering  
Jilin University  
2699 Qianjin Street  
Changchun, 130012, PR China  
E-mail: yonglaizhang@jlu.edu.cn; hbsun@jlu.edu.cn  
Prof. H.-B. Sun  
College of Physics, Jilin University  
119 Jiefang Road, Changchun, 130023, PR China



DOI: 10.1002/adom.201300401



**Scheme 1.** Schematic illustration of the FsLDW system used for programmable N-doping and reduction of GO.

rare. Here, for the first time, we demonstrate programmable N doping and the simultaneous reduction of GO by femtosecond laser direct writing (FsLDW) in  $\text{NH}_3$  atmosphere. Complex micropatterns of N-doped and reduced GO (NRGO) have been successfully fabricated towards device fabrication. We further investigate the effect of laser power on the N-doping efficiency/N-bonding types both experimentally and theoretically, a total nitrogen concentration as high as 10.3% in the form of pyridinic, pyrrolic, and graphitic has been achieved. As a proof-of-concept, bottom-gate n-type graphene FETs have been post-fabricated by direct writing an NRGO channel between pre-patterned source/drain electrodes. The laser-mediated programmable N-doping and simultaneous reduction of GO holds great promise for manufacturing complicated architectures such as logic gates and p-n diodes towards the flexible fabrication and integration of cost-effective graphene electronics.

The processing system for FsLDW-mediated N-doping and reduction of GO is shown in **Scheme 1**, a spin-coated GO film either on a glass slice or on a flexible PET substrate was mounted on a piezo moving stage with nanometer-motion accuracy, controlled by a computer according to the pre-programmed micropatterns. To accomplish the FsLDW in  $\text{NH}_3$  atmosphere, the GO film was tightly covered by a hemispheric cavity with an inlet connected to the  $\text{NH}_3$  source and an outlet connected to an acid recycle pool. In this way, a focused femtosecond laser directly scanned the GO film as the computer was programmed. Since the reduction and doping can only occur in the area irradiated by laser focus, high-resolution micropatterns of NRGO could be readily fabricated. As shown in **Figure 1**, a series of complex micropatterns including bow-like microcircuits, involute-like microcircuits, letters, electrodes, involute-like microcircuits, and a hexagon grid.

and even the badge of Jilin University could be successfully created. The optical microscopy image of the micropatterns can be clearly identified due to the difference in transmittance between GO and NRGO regions. Figure S1 in the Supporting Information shows the transmittance of GO and NRGO films prepared under different laser powers on quartz substrates. The NRGO films are less transparent than the GO film in visible range. This darkening of the reduced region has been observed previously, which could be attributed to the partial restoration of the  $\pi$ -electron system in the GO.<sup>[17]</sup> In addition to glass substrates, a typical NRGO electrode array was fabricated on a flexible PET substrate (Figure 1i). This arbitrary patterning of N-doped graphene shows great advantages for the fabrication of graphene-based electronics, especially for flexible devices, because any desired micropatterns of RGO or NRGO can be integrated flexibly by this FsLDW technique.

To get further insight into the surface topography, an araneose micropattern of NRGO has been selected as a representative example for atomic force microscopy (AFM) characterization. As shown in **Figure 2**, the araneose micropattern could be clearly identified from the GO film. After FsLDW-mediated N-doping and simultaneous removal of oxygen-containing

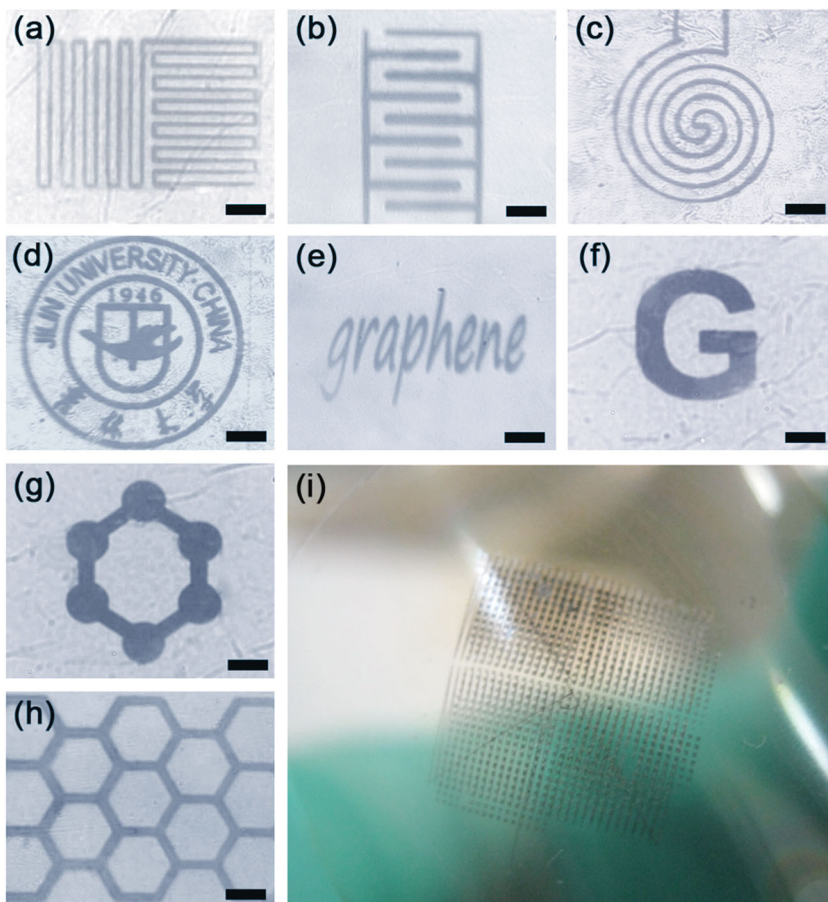


**Figure 1.** Optical microscopy images of NRGO micropatterns. (a) Bow-like microcircuit, (b) comb-like electrodes, (c) involute-like microcircuit, (d) the badge of Jilin University, (e) the word "graphene", (f) the letter "G", (g) the molecular structure of a benzene, and (h) a hexagon grid. Scale bars are 10  $\mu\text{m}$ . (i) Photograph of a typical NRGO electrode array on a flexible PET substrate.

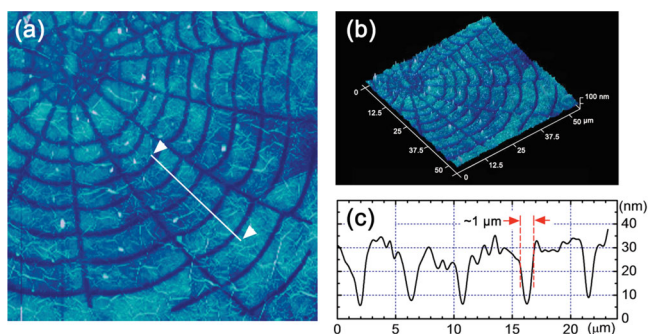


**Figure 2.** (a) 2D and (b) 3D AFM images of an araneose NRGO micropattern; (c) height profile along the white line in (a).

groups (OCGs), a sunken surface was formed in the laser scanned region. This phenomenon has also been observed in the laser reduction of GO which has been previously reported by our groups and others.<sup>[15,16]</sup> The reason for the sunken surface could be attributed to the mass loss of OCGs in the form of CO<sub>2</sub>, CO, H<sub>2</sub>O and carbon species. However, there are also some papers reporting an increased film thickness after the laser irradiation due to the formation of a porous structure.<sup>[18]</sup> The inconsistency of surface topologies could be ascribed to the use of a femtosecond laser. Since the femtosecond laser pulse duration is very short, even shorter than the electron cooling time, heat diffusion is minimized. During femtosecond laser direct writing, the material changes from a solid state to a plasma state with a high temperature and pressure instantaneously, leading to gases spraying from the substrate rapidly, while the surrounding material is still in the “cold state”. In this regard, femtosecond laser reduction can effectively avoid the accumulation and expansion of the generated gases, and thus give rise to a flat and sunken surface. Figure 2c shows the height profile along the white line marked in Figure 2a. The line width was measured to be ~1 μm; and the sunken depth is about 20 nm when the laser power is 10 mW.

The presence of N species in the NRGO was confirmed by X-ray photoelectron spectroscopy (XPS). In our work, the preparation of NRGO was implemented under three laser powers,

8 mW, 10 mW, and 12 mW. Survey X-ray photoelectron spectra of the three samples show the introduction of nitrogen species and the removal of OCGs (Figure S2, Supporting Information). Notably, pristine GO is very rich in oxygen, more than 53%; after laser treatment in NH<sub>3</sub> atmosphere, the oxygen content decreased significantly with the increase of laser power, indicating the reduction of GO. Additionally, 3.1%, 10.3%, and 9.1% of nitrogen have been detected for NRGO samples prepared under laser powers of 8 mW, 10 mW, and 12 mW, respectively, suggesting the effective N-doping of graphene. Here, the NH<sub>3</sub> pressure inside the polydimethylsiloxane (PDMS) cavity is maintained at atmospheric pressure. In fact, the N-doping level could also be controlled by changing the partial pressure of NH<sub>3</sub>. When the partial pressure of NH<sub>3</sub> is reduced to 40% (60% of N<sub>2</sub>), the nitrogen contents decreased to 2.6% from 9.1% (Figure S2). The reduction of GO under higher NH<sub>3</sub> pressure is expected to achieve higher doping levels, however, considering the fact that both the substrates (coverslip, ~200 μm in thickness) and the thin PDMS cavity can not bear high pressure, N-doping under higher NH<sub>3</sub> pressure has not been carried out.

To evaluate the doping type of the nitrogen species, we also tested the stability of the NRGO samples. As reported elsewhere, nitrogen species could be doped in GO through physical adsorption, fusing, and covalent bonding.<sup>[19]</sup> In our work, we treated our NRGO sample under vacuum at 150 °C for 3 h. Figure S3 shows the survey X-ray photoelectron spectra of NRGO samples before and after vacuum heat treatment. Only a slight decrease in oxygen (from 28.4% to 25.3%) could be observed due to the thermal deoxidizing of the residual oxygen-containing groups. The concentration of nitrogen almost kept the same value (slightly increased due to the loss of oxygen), indicating that the doping is stable and irreversible.

Figure 3a shows the C1s XPS spectra of GO and NRGO samples, the C1s spectra have been deconvoluted using four Gaussian peaks that correspond to C–C (284.6 eV), C–N (285.8 eV), C–O (286.6 eV), and C=O (288.5 eV), respectively. For pristine GO sample, no N signal has been detected and C–C content is only 42.1%. After laser irradiation, oxygen signals decreased significantly, indicating the reduction of GO. The contents of C,

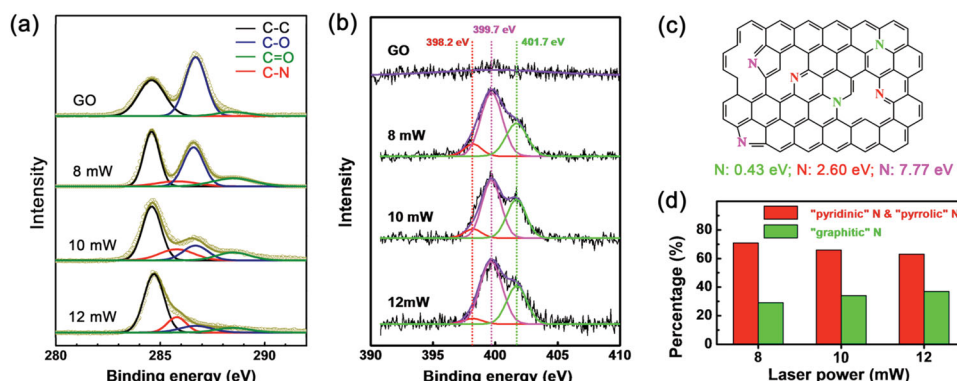


**Figure 3.** (a) C1s XPS spectra of pristine GO and NRGO prepared under different laser powers; (b) N1s spectra of pristine GO and NRGO prepared under different laser powers; the N1s peak can be fitted into three peaks at 398.2, 399.7 and 401.7 eV, which are labeled pyridinic-, pyrrolic-, and graphitic-N, respectively; (c) schematic representation of the N-doped graphene and the corresponding formation energy calculated from first principle study; (d) dependence of the percentage of pyridinic-/pyrrolic- and graphitic-N on laser power.

**Table 1.** Elemental contents and the percentage of different carbon bonds.<sup>a)</sup>

Samples	Laser power [mW]	C [%]	O [%]	N [%]	C–C [%]	C–O [%]	C=O [%]	C–N [%]
GO	–	46.5	53.5	–	42.1	52.2	5.7	–
NRGO-8	8	44.1	52.8	3.1	38.9	35.7	16.4	9.0
NRGO-10	10	54.5	35.2	10.3	50.2	18.1	12.9	18.8
NRGO-12	12	75.3	15.6	9.1	64.2	11.3	8.7	15.8

<sup>a)</sup>The values are calculated from XPS results.

O, and N, as well as the percentages of different carbon bonds have been summarized in **Table 1**. The highest N concentration of 10.3% has been achieved when the laser power is 10 mW; and the percentage of C–N is as high as 18.8%.

The analysis of the nitrogen chemical environment is shown in Figure 3b, where N1s XPS spectra of NRGO samples have been deconvoluted into three peaks at 398.2, 399.7, and 401.7 eV, which could be attributed to pyridinic-, pyrrolic- and graphitic-N, respectively. Figure 3c shows a schematic illustration of the N-doped graphene and the corresponding formation energy of different N species calculated from the first principles study (for details of the calculation, see the Supporting Information). Notably, the formation energy of graphitic-N is much lower than that of pyridinic- and pyrrolic-N. However, for the NRGO samples, more than half of the N atoms are doped in the form of pyrrolic-N. This result suggests that the oxygen containing groups (OCGs) and defects in GO facilitate the formation of pyrrolic-N during the laser irradiation. The hypothesis has also been confirmed by our experimental results. With the increase of laser power, the peak for graphitic-N increased gradually, which indicates that more N atoms are substitutionally doped into the graphene lattice mainly in the form of graphitic N at a higher laser power. For instance, when the laser power is 12 mW, most of the OCGs could be removed effectively; as a result, the total N content decreased to 9.1% as compared with NRGO-10 mW (10.3%), whereas the relative graphitic N increased slightly. Figure 3d presents the dependence of pyridinic-/pyrrolic- and graphitic-N contents on laser power. According to the results reported in Usachov's work,<sup>[7d]</sup> the graphitic-N contributes mainly to the n-type behavior instead of the pyridinic-/pyrrolic-N. In this regard, processing at a higher laser power would facilitate the n-type tuning by introducing more graphitic-N. However, we found that further increasing the laser power partly destroys the NRGO film due to a laser ablation effect.

To evaluate the structural changes before and after N-doping and the reduction of GO, Raman spectra were measured over both GO and NRGO samples (Figure S4, Supporting Information). Generally, the intensity ratio of the D band (1350 cm<sup>-1</sup>) to the G band (1580 cm<sup>-1</sup>) ( $I_D/I_G$ ) is used to estimate

the disorder of graphene. However, for our NRGO samples, the  $I_D/I_G$  ratio only slightly increased as compared with pristine GO. It is known that the intensity of the G band should enhance on the assumption that the sp<sup>2</sup> domain has been partly restored due to the effective reduction, so the nonobvious increase in the  $I_D/I_G$  ratio should be attributed to the doping of N-species, which brings additional defects to the graphene structure. The 2D peak (the second order of the D-peak, at ~2700 cm<sup>-1</sup>) is the most intrinsic to graphene as compared to bulk graphite. It arises as a result of a two-phonon resonance process, involving phonons near the K point. For our NRGO sample, a very small 2D band could be detected in the Raman spectra; it could be attributed to the presence of defects in the basal plane and a variety of functional groups terminating the edges.

As a proof-of-concept, n-type FETs were post-fabricated by direct writing an NRGO channel between two pre-patterned source/drain electrodes. The thickness of the Au electrodes is about 100 nm. It is worth pointing out that, in the whole fabrication procedure, the NRGO channel could be created flexibly in the last step, indicating the “post-integration” feature. Since the

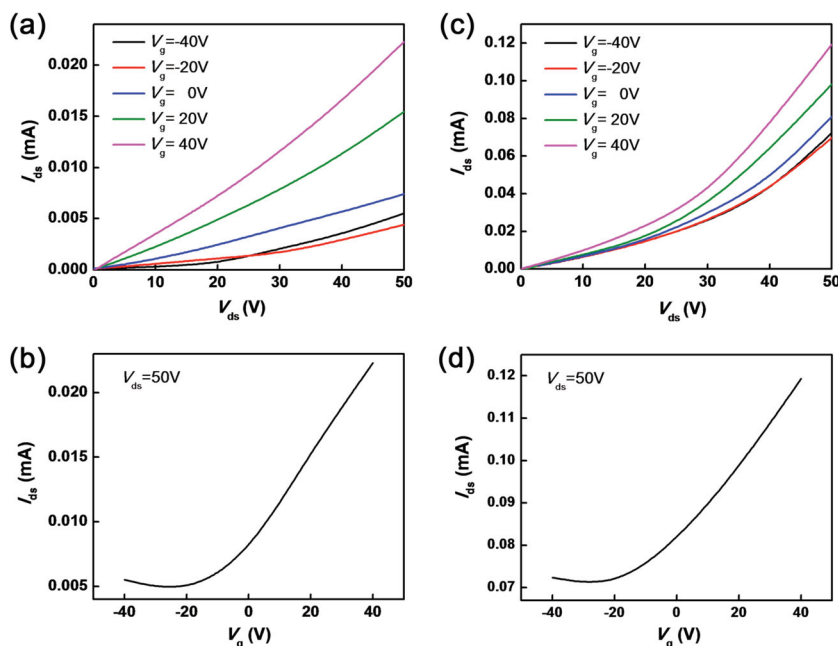


**Figure 4.** Output and transfer characteristics of NRGO FETs with (a,b) NRGO (8 mW) and (c,d) NRGO (10 mW) as channels. When  $V_{ds} = 50$  V, the hole mobilities are 0.38 and 1.1 cm<sup>2</sup> V<sup>-1</sup> s<sup>-1</sup>, and the  $I_{on}/I_{off}$  ratios are 5.0 and 1.7, respectively.

laser power used for GO treatment is only 12 mW—not high enough to cause damage of Au electrodes—we extended the laser scanning path into the Au/GO contact region to ensure a reliable ohmic contact. **Figure 4** shows the output and transfer curve of the FETs fabricated under laser powers of 8 and 10 mW, respectively. As shown in **Figure 4a**, the FET fabricated at 8 mW shows an  $I_{\text{on}}/I_{\text{off}}$  ratio of 5.0 with an estimated electron mobility of  $0.38 \text{ cm}^2 \text{ V}^{-1} \text{ s}^{-1}$  (for detail calculations, see the Supporting Information). When the laser power is increased to 10 mW, the conductivity and the carrier density of the channel becomes higher (electron mobility of  $1.1 \text{ cm}^2 \text{ V}^{-1} \text{ s}^{-1}$ ), due to the combined effect of OCG removal and N-doping. Additionally, more graphitic-N could provide more free electrons, giving rise to higher conductivity. **Figure 4b,d** show the transfer characteristics of the FETs; the neutrality point of NRGO was at negative gate voltages of  $V_{\text{gs}} \sim -20 \text{ V}$ , indicating the n-type electron doping behavior. The majority carrier in the NRGO channel is the electron, which is different from the FET fabricated in air, as we reported previously.<sup>[15a]</sup>

In conclusion, a programmable N-doping and simultaneous reduction of GO have been achieved by FsLDW of GO in ammonia atmosphere. The unique laser-mediated N-doping of RGO permits exquisite control over the doping area, therefore making it possible to fabricate complex micropatterns on both glass and polymer substrates. By tuning the laser power, from 8 mW to 12 mW, both N-doping concentration and the bond types of N species could be modulated; the highest nitrogen concentration of 10.3% has been achieved. Based on our experimental results and the first principles study, we found that the OCGs and defects on the GO sheets are responsible for N-doping in the form of pyridinic- and pyrrolic-N, and an increase in laser power would enhance the content of graphitic-N. As a proof-of-concept, a bottom-gate n-type graphene FET has been post-fabricated by direct writing an NRGO channel between pre-patterned source/drain electrodes, demonstrating the great potential for the flexible fabrication and integration of graphene-based devices. N-type transistor behavior has been observed due to the effective N-doping.

## Experimental Section

**Laser-Mediated N-Doping and Reduction of GO in  $\text{NH}_3$  Atmosphere:** GO was produced via the Hummers method from natural graphite (Aldrich,  $< 150 \mu\text{m}$ ). The GO films were prepared by spin-coating GO solution at 2000 rpm for 20 s on glass substrates which had been cleaned by ethanol and dried in vacuum at  $95 \text{ }^\circ\text{C}$  for 1 h. The  $\text{NH}_3$  atmosphere is supplied by a PDMS hemispherical cavity that tightly covers the glass substrates. Two air vent needle plugged in the cavity are inlet and outlet of pure  $\text{NH}_3$ . The  $\text{NH}_3$  pressure inside the PDMS cavity is maintained at atmospheric pressure. For the fabrication under low  $\text{NH}_3$  partial pressure (40%), 60% of  $\text{N}_2$  was mixed. Pulses from a femtosecond laser oscillator of 800 nm central wavelength, 120 fs pulse duration, and 80 MHz repetition rate, were tightly focused by a 100 $\times$  oil immersion objective lens with a high numerical aperture (NA) of 1.35 into the GO film. The focal spot of the laser beam was scanned laterally by steering a two-galvano-mirror set and was vertically moved along the optical axis by a piezo stage. Scanning mode of the laser processing is point to point, 600  $\mu\text{s}$  exposure duration of each voxel and 200 nm scanning step length were adopted for the processing. Then the femtosecond laser directly wrote on the GO film according to preprogrammed patterns designed by a computer.

**Fabrication and Measurement of NRGO FETs:** For the fabrication of FETs, the ITO gate electrode was sputtered onto the substrates through a shadow mask. Then poly(methyl methacrylate) (PMMA) chloroform solution (0.1 g/mL) was spin-coated on the ITO substrates at 3000 rpm and baked at  $95 \text{ }^\circ\text{C}$  for 15 min as a gate dielectric layer. The thickness of PMMA is measured to be 200 nm. GO films were spin-coated on PMMA layer and annealed at  $95 \text{ }^\circ\text{C}$  for 1 h. Au source and drain electrodes were vaporized onto the GO film under vacuum by using a shadow mask. The film was then covered tightly by a PDMS cavity with air inlet and outlet.  $\text{NH}_3$  flows into the cavity. GO film was then reduced and patterned into a 30  $\mu\text{m}$  width belt between the electrodes (distance, 20  $\mu\text{m}$ ) for test.

**Characterization:** X-ray photoelectron spectroscopy (XPS) was performed using an ESCALAB 250 spectrometer. Atomic force microscopy (AFM) images were measured with Digital Instruments NanoScope IIIa. Optical microscope images were obtained from a Motic BE400 microscope. Current–voltage curves of FET were measured from a Keithley SCS 4200 semiconductor characterization system. Raman spectra were measured with a Renishaw Raman microscope using 514 nm wavelength laser.

## Supporting Information

Supporting Information is available from the Wiley Online Library or from the author.

## Acknowledgements

The authors gratefully acknowledge support from National Basic Research Program of China. Grant Number: 2011CB013000; NSFC (Grant Nos. 61376123, 61008014, 90923037, 6078048 and 11104109), We also acknowledge the China Postdoctoral Science Foundation No. 2013M530140 and the High Performance Computing Center at JLU for computing resources.

Received: September 25, 2013

Revised: November 10, 2013

Published online: December 2, 2013

- [1] a) A. K. Geim, K. S. Novoselov, *Nat. Mater.* **2007**, *6*, 183; b) A. K. Geim, *Science* **2009**, *324*, 1530; c) Y. B. Zhang, Y. W. Tan, H. L. Stormer, P. Kim, *Nature* **2005**, *438*, 201; d) K. S. Novoselov, A. K. Geim, S. V. Morozov, D. Jiang, Y. Zhang, S. V. Dubonos, I. V. Grigorieva, A. A. Firsov, *Science* **2004**, *306*, 666.
- [2] a) J. B. Oostinga, H. B. Heersche, X. L. Liu, A. F. Morpurgo, L. M. K. Vandersypen, *Nat. Mater.* **2008**, *7*, 151; b) L. Liao, J. W. Bai, Y. C. Lin, Y. Q. Qu, Y. Huang, X. F. Duan, *Adv. Mater.* **2010**, *22*, 1941.
- [3] a) P. K. Ang, W. Chen, A. T. S. Wee, K. P. Loh, *J. Am. Chem. Soc.* **2008**, *130*, 14392; b) Q. M. Ji, I. Honma, S. M. Paek, M. Akada, J. P. Hill, A. Vinu, K. Ariga, *Angew. Chem. Int. Ed.* **2010**, *49*, 9737; c) J. L. Johnson, A. Behnam, S. J. Pearton, A. Ural, *Adv. Mater.* **2010**, *22*, 4877; d) Y. Ohno, K. Maehashi, K. Matsumoto, *J. Am. Chem. Soc.* **2010**, *132*, 18012.
- [4] T. Mueller, F. N. A. Xia, P. Avouris, *Nat. Photonics* **2010**, *4*, 297.
- [5] a) V. Barone, O. Hod, G. E. Scuseria, *Nano Lett.* **2006**, *6*, 2748; b) Y. W. Son, M. L. Cohen, S. G. Louie, *Phys. Rev. Lett.* **2006**, *97*, 216803.
- [6] J. W. Bai, X. Zhong, S. Jiang, Y. Huang, X. F. Duan, *Nat. Nanotechnol.* **2010**, *5*, 190.
- [7] a) L. S. Panchokarla, K. S. Subrahmanyam, S. K. Saha, A. Govindaraj, H. R. Krishnamurthy, U. V. Waghmare, C. N. R. Rao, *Adv. Mater.* **2009**, *21*, 4726; b) T. B. Martins, R. H. Miwa,

- A. J. R. da Silva, A. Fazio, *Phys. Rev. Lett.* **2007**, *98*; c) L. Y. Zhao, R. He, K. T. Rim, T. Schiros, K. S. Kim, H. Zhou, C. Gutierrez, S. P. Chockalingam, C. J. Arguello, L. Palova, D. Nordlund, M. S. Hybertsen, D. R. Reichman, T. F. Heinz, P. Kim, A. Pinczuk, G. W. Flynn, A. N. Pasupathy, *Science* **2011**, *333*, 999; d) D. Usachov, O. Vilkov, A. Gruneis, D. Haberer, A. Fedorov, V. K. Adamchuk, A. B. Preobrajenski, P. Dudin, A. Barinov, M. Oehzelt, C. Laubschat, D. V. Vyalikh, *Nano Lett.* **2011**, *11*, 5401.
- [8] a) Y. W. Zhang, J. Ge, L. Wang, D. H. Wang, F. Ding, X. M. Tao, W. Chen, *Sci. Rep.* **2013**, *3*, 2771; b) H. B. Wang, T. Maiyalagan, X. Wang, *ACS Catal.* **2012**, *2*, 781.
- [9] D. C. Wei, Y. Q. Liu, Y. Wang, H. L. Zhang, L. P. Huang, G. Yu, *Nano Lett.* **2009**, *9*, 1752.
- [10] X. R. Wang, X. L. Li, L. Zhang, Y. Yoon, P. K. Weber, H. L. Wang, J. Guo, H. J. Dai, *Science* **2009**, *324*, 768.
- [11] B. D. Guo, Q. A. Liu, E. D. Chen, H. W. Zhu, L. A. Fang, J. R. Gong, *Nano Lett.* **2010**, *10*, 4975.
- [12] X. L. Li, H. L. Wang, J. T. Robinson, H. Sanchez, G. Diankov, H. J. Dai, *J. Am. Chem. Soc.* **2009**, *131*, 15939.
- [13] N. A. Kumar, H. Nolan, N. McEvoy, E. Rezvani, R. L. Doyle, M. E. G. Lyons, G. S. Duesberg, *J. Mater. Chem. A* **2013**, *1*, 4431.
- [14] a) K. S. Subrahmanyam, P. Kumar, A. Nag, C. N. R. Rao, *Solid State Commun.* **2010**, *150*, 1774; b) P. Kumar, K. Subrahmanyam, C. Rao, *Int. J. Nanoscience* **2011**, *10*, 559; c) P. Kumar, K. S. Subrahmanyam, C. N. R. Rao, *Mater. Express* **2011**, *1*, 252; d) P. Kumar, B. Das, B. Chitara, K. S. Subrahmanyam, K. Gopalakrishnan, S. B. Krupanidhi, C. N. R. Rao, *Macromol. Chem. Phys.* **2012**, *213*, 1146; e) K. S. Subrahmanyam, P. Kumar, U. Maitra, A. Govindaraj, K. P. S. S. Hembram, U. V. Waghmare, C. N. R. Rao, *Proc. Natl. Acad. Sci. USA* **2011**, *108*, 2674; f) K. Gopalakrishnan, K. S. Subrahmanyam, P. Kumar, A. Govindaraj, C. N. R. Rao, *RSC Adv.* **2012**, *2*, 1605.
- [15] a) L. Guo, R. Q. Shao, Y. L. Zhang, H. B. Jiang, X. B. Li, S. Y. Xie, B. B. Xu, Q. D. Chen, J. F. Song, H. B. Sun, *J. Phys. Chem. C* **2012**, *116*, 3594; b) Y. L. Zhang, L. Guo, S. Wei, Y. Y. He, H. Xia, Q. D. Chen, H. B. Sun, F. S. Xiao, *Nano Today* **2010**, *5*, 15.
- [16] a) Y. Zhou, Q. L. Bao, B. Varghese, L. A. L. Tang, C. K. Tan, C. H. Sow, K. P. Loh, *Adv. Mater.* **2010**, *22*, 67; b) V. Strong, S. Dubin, M. F. El-Kady, A. Lech, Y. Wang, B. H. Weiller, R. B. Kaner, *ACS Nano* **2012**, *6*, 1395; c) D. A. Sokolov, C. M. Rouleau, D. B. Geohegan, T. M. Orlando, *Carbon* **2013**, *53*, 81; d) H. F. Teoh, Y. Tao, E. S. Tok, G. W. Ho, C. H. Sow, *J. Appl. Phys.* **2012**, *112*, 064309; e) P. Kumar, *RSC Adv.* **2013**, *3*, 11987; f) Y. L. Zhang, L. Guo, H. Hong, Q. D. Chen, J. Feng, H. B. Sun, *Adv. Opt. Mater.* **2013**, DOI: 10.1002/adom.201300317.
- [17] a) H. A. Becerril, J. Mao, Z. Liu, R. M. Stoltenberg, Z. Bao, Y. Chen, *ACS Nano* **2008**, *2*, 463; b) S. Stankovich, D. A. Dikin, G. H. B. Dommett, K. M. Kohlhaas, E. J. Zimney, E. A. Stach, R. D. Piner, S. T. Nguyen, R. S. Ruoff, *Nature* **2006**, *442*, 282.
- [18] a) M. F. El-Kady, V. Strong, S. Dubin, R. B. Kaner, *Science* **2012**, *335*, 1326; b) W. Gao, N. Singh, L. Song, Z. Liu, A. L. M. Reddy, L. J. Ci, R. Vajtai, Q. Zhang, B. Q. Wei, P. M. Ajayan, *Nat. Nanotechnol.* **2011**, *6*, 496.
- [19] a) Z. T. Luo, N. J. Pinto, Y. Davila, A. T. C. Johnson, *Appl. Phys. Lett.* **2012**, *100*, 253108; b) A. Tiberj, M. Rubio-Roy, M. Paillet, J. R. Huntzinger, P. Landois, M. Mikolasek, S. Contreras, J. L. Sauvajol, E. Dujardin, A. A. Zhabab, *Sci. Rep.* **2013**, *3*, 2355.